

PoseGaussian: Pose-Driven Novel View Synthesis for Robust 3D Human Reconstruction

Ju Shen¹ Chen Chen² Tam V. Nguyen¹ Vijayan K. Asari¹

¹University of Dayton

²University of Central Florida

jshen1@udayton.edu, chen.chen@crcv.ucf.edu, tnguyen1@udayton.edu, vasari1@udayton.edu

Abstract

We propose PoseGaussian, a pose-guided Gaussian Splatting framework for high-fidelity human novel view synthesis. Human body pose serves a dual purpose in our design: as a structural prior, it is fused with a color encoder to refine depth estimation; as a temporal cue, it is processed by a dedicated pose encoder to enhance temporal consistency across frames. These components are integrated into a fully differentiable, end-to-end trainable pipeline. Unlike prior works that use pose only as a condition or for warping, PoseGaussian embeds pose signals into both geometric and temporal stages to improve robustness and generalization. It is specifically designed to address challenges inherent in dynamic human scenes, such as articulated motion and severe self-occlusion. Notably, our framework achieves real-time rendering at 100 FPS, maintaining the efficiency of standard Gaussian Splatting pipelines. We validate our approach on ZJU-MoCap, THuman2.0, and in-house datasets, demonstrating state-of-the-art performance in perceptual quality and structural accuracy (PSNR 30.86, SSIM 0.979, LPIPS 0.028).

1. Introduction

Novel View Synthesis (NVS) is a fundamental problem in computer vision and graphics, crucial for applications such as virtual reality and telepresence. It has evolved from traditional image-based rendering (IBR) techniques [14, 55, 91] to advanced neural representations like Neural Radiance Fields (NeRF) [46] and their extensions [58, 70, 83], achieving impressive realism in view generation. This advancement has sparked growing interest in free-viewpoint human rendering, an important NVS subfield. Nevertheless, synthesizing high-quality human views remains difficult due to dynamic motion, individual appearance variations, and real-time constraints. Recent works have adapted

NeRF frameworks to capture human appearance and motion [54, 68]. Although effective in modeling person-specific details, the implicit volumetric rendering approach—which requires dense spatial sampling—creates a bottleneck for real-time applications.

Recent advances in 3D Gaussian Splatting (3D-GS) have demonstrated impressive runtime performance while maintaining high visual fidelity [33]. Unlike NeRF, 3D-GS adopts an explicit functional representation that enables direct projection of Gaussian primitives, making it well-suited for real-time applications. This paradigm has shown strong potential in domains such as free-viewpoint human rendering [23, 34, 90]. Despite these successes, existing methods largely rely on low-level appearance cues and struggle to handle complex human motions. For instance, while GPS-Gaussian [90] demonstrates real-time human view synthesis, it does not incorporate explicit human semantics—such as pose or body structure—into the prediction of Gaussian parameters. On the other hand, GauHuman [23] introduces structured human priors into the pipeline by leveraging fits from SMPL (Skinned Multi-Person Linear Model) [44] to guide Gaussian generation. However, its strong reliance on accurate SMPL alignment limits generalization in the presence of pose noise or when body shapes deviate from the training distribution. Moreover, it struggles with rapid motion, often producing motion blur and background leakage.

To bridge the gap between low-level Gaussian representations and the effective integration of human priors, we introduce a pose-guided 3D-GS representation that incorporates body pose and temporal dynamics directly into the rendering pipeline. This structured prior provides strong semantic anchoring and enhances temporal coherence, particularly under sparse views or rapid motion. Figure 1 (left) illustrates the core concept of our method—reconstructing a pose-guided motion sequence and reprojecting it into the scene—showing how extracted pose priors guide coherent temporal updates. Figure 1 (right) presents a quantitative

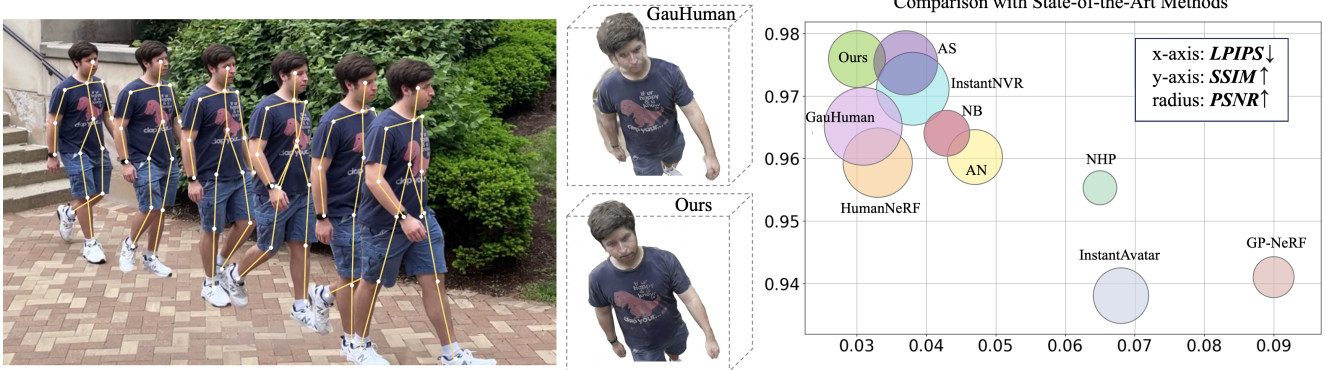


Figure 1. **PoseGaussian Visualization and Comparison.** Left: reconstructed pose-guided motion sequence reprojected into the original scene. Middle: visual comparison with GauHuman [23]. Right: performance chart compared to selected methods on the three metrics LPIPS, SSIM, PSNR. Compared methods: GauHuman ([23]), AS [92], InstantNVR [17], HumanNeRF [88], NB [53], AN [52], NHP [35], InstantAvatar [29], GP-NeRF [10].

comparison against recent state-of-the-art methods on the standard public benchmark ZJU-MoCap [54], where our approach consistently achieves superior performance across the three metrics—PSNR [25], SSIM [74], and LPIPS [85]. To emphasize the perceptual sharpness and structural fidelity of our results, Figure 1 (middle) visualizes reconstructed novel views alongside GauHuman [23], which exhibits motion blur and unclear boundaries under dynamic motion. Our main contributions are as follows:

- **Pose-aware initialization scheme** that leverages human body priors to guide the estimation of Gaussian primitives, enabling semantically informed and structurally coherent representations.
- **Temporal regularization strategy** that promotes inter-frame consistency while preserving fine-grained details and accommodating natural motion variations.
- **End-to-end differentiable framework** that jointly incorporates pose-informed feature encoding and motion-consistent regularization within a unified architecture for dynamic human reconstruction.

Our approach achieves state-of-the-art performance on several benchmark datasets, demonstrating superior reconstruction quality, enhanced temporal stability, and real-time rendering efficiency compared to existing methods.

2. Related Works

Human view synthesis has evolved from early 3D reconstruction using structured light and laser scanning, to model-driven methods like SCAPE [3] and SMPL [44], which represent human bodies with articulated models. Though influential, these methods often lacked photorealism and required strong priors or manual tuning. More

recently, learning-based techniques such as Neural Radiance Fields (NeRF) [46] have enabled photorealistic novel view synthesis directly from images. Building on this, 3D-GS [33] introduces an explicit, point-based representation using 3D Gaussians to improve rendering efficiency. We focus on this modern paradigm for human appearance reconstruction.

Radiance Fields and Human Representation: NeRF has been extended to human subjects with minimal motion [38, 50, 51], enabling view synthesis without explicit motion modeling. Several methods incorporate parametric human models like SMPL [44] or 3D skeletons [52, 54, 83] to support pose-conditioned rendering. Neural Body [54] and Neural Actor [42] apply sparse convolutions and mesh-based warping, but often require per-subject optimization and generalize poorly to unseen poses. Others, such as HumanNeRF [78] and Vid2Actor [77], focus on single-video rendering, yet struggle to capture fine details without dense supervision. Dynamic scenarios further expose limitations in pose estimation and warping, often resulting in artifacts like flickering and jittering [42, 52]. Overall, implicit volumetric NeRF models remain computationally heavy and memory-intensive, with slow training and inference. While acceleration techniques exist [15, 19], the implicit nature still impedes scalability and real-time use.

Gaussian Splatting for Human Novel View Synthesis: 3D-GS [33] has quickly become a leading direction for human-centric representations, sparking a wave of influential work [23, 34, 37, 47, 49, 59, 65]. One growing line of research explores sparse-camera setups to improve efficiency and training speed [12, 90], which are promising for real-time applications but may struggle with capturing fine-grained geometry or detailed motion. For example, GPS-Gaussian [90] omits explicit human modeling, while HF-Gaussian [12] relies on depth maps predicted from RGB,

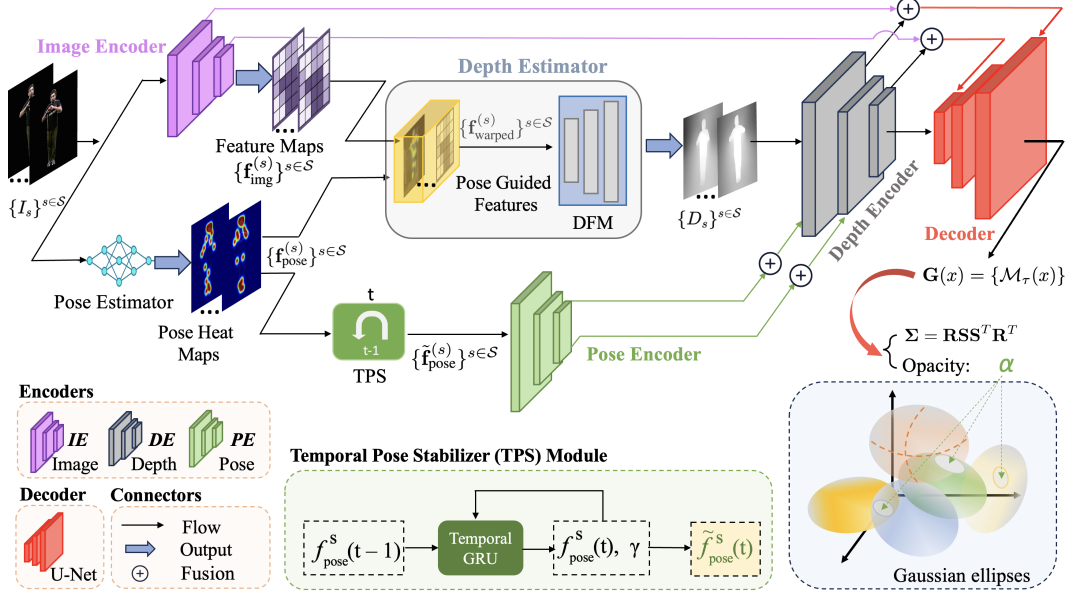


Figure 2. The PoseGaussian pipeline. *Top*: The overall workflow, illustrating the process from input color images to the predicted Gaussian parameter maps, specifically the rotation $\mathcal{M}_r(x)$, scale $\mathcal{M}_s(x)$, and opacity $\mathcal{M}_\alpha(x)$. *Bottom*: A detailed view of the Temporal Pose Stabilizer (TPS) module, along with visual annotations clarifying the roles of various modules and connections.

potentially introducing temporal artifacts. Another prominent direction combines Gaussian Splatting with parametric body models like SMPL, typically using Linear Blend Skinning (LBS) [31], to achieve more accurate and controllable dynamic human representations [23, 34, 37, 47, 49, 65]. While this improves realism, it often depends on fixed body templates and complex pipelines, limiting generalization across diverse identities and motion types [34, 65]. Our method bridges both directions with a lightweight, model-free design that introduces human structure via sparse 3D pose cues, retaining efficiency while improving stability and adaptability across varied motions and appearances.

3. The PoseGaussian Method

Fig. 2 illustrates the overall architecture, which comprises three primary encoders: an image encoder (IE) for extracting dense visual features, a pose encoder (PE) for interpreting skeletal keypoint distributions, and a depth encoder (DE) for estimating scene geometry. The pipeline takes input images processed by the IE and fuses pose heatmaps from a pre-trained estimator with image features, providing the DE with human-centric cues to improve scene geometry. In parallel, the keypoint heatmaps are further processed through a Temporal Pose Stabilizer (TPS) module and subsequently encoded by the PE. The resulting pose features are decoded with the help of joint skip connections to reinforce temporal consistency and preserve semantic details. The final output consists of pixel-aligned 2D Gaussian parameter maps $\mathbf{G}(x) = \mathcal{M}_\tau(x)$, where $\tau \in \{p, c, r, s, \alpha\}$.

denotes the projected position, color, rotation, scale, and opacity at each pixel location x . While 3D Gaussians provide stronger view consistency, our choice of 2D primitives avoids explicit 3D reconstruction and allows for more flexible modeling of image-space variations, which aligns better with our pose-conditioned, mesh-free formulation.

3.1. Pose-Guided Feature Fusion for Depth Inference

To improve geometric accuracy under motion, we leverage pose priors that inform the visual representation by introducing semantically aligned structural guidance. Simple pose heatmaps—such as those from BlazePose [5]—are lightweight, resolution-aligned, and readily compatible with the PE, making them well-suited for this purpose. Our method is compatible with various pose estimation backbones: when pose data is available in different formats (e.g., from prior works on robust pose estimation [43, 89]), joints can be projected and encoded as 3D Gaussian heatmaps via joint-to-heatmap encoding. While our current implementation uses RAFT-Stereo for improved depth in binocular setups, PoseGaussian can also be adapted to monocular sequences by substituting the depth module with monocular estimators or omitting depth cues entirely, enabling pose-conditioned generation from single-view sources [60]. Future work will examine how the accuracy and nature of the pose estimation backbone affect final reconstruction quality.

From each source view $s \in \mathcal{S}$, two types of features are obtained: image features are extracted using a convo-

lutional encoder, while pose features are generated directly by a pose estimation network [5].

$$\mathbf{f}^{(s)} = \begin{cases} \mathbf{f}_{\text{img}}^{(s)} = \mathcal{E}_{\text{img}}(I_s) \in \mathbb{R}^{H/2^k \times W/2^k \times D_i}, \\ \mathbf{f}_{\text{pose}}^{(s)} = P_s \in \mathbb{R}^{H/2^k \times W/2^k \times D_p} \end{cases} \quad (1)$$

where P_s and I_s are the 2D pose and RGB image from the s -th source view. The spatial resolution $H/2^k \times W/2^k$ reflects the output size after k stages of downsampling in the encoder, with $k = 3$ or 4 in our implementation. Here, D_i and D_p denote the channel dimensions for the image and pose features, respectively. The two streams are fused along the channel dimension to form the unified feature map $\mathbf{f}^{(s)}$, where simple concatenation or alternative fusion strategies (e.g., [20, 67]), as discussed in the ablation study. The fused feature set $\{\mathbf{f}^{(s)}\}_{s \in \mathcal{S}}$ is first warped to the target view using the corresponding extrinsics and estimated depth from the DE module, producing the warped feature representation $\{\mathbf{f}_{\text{warped}}^{(s)}\}_{s \in \mathcal{S}}$. Following the design of RAFT-Stereo [41], we construct a correlation-based feature volume by aggregating view-wise similarities between the warped source features $\mathbf{f}_{\text{warped}}^{(s)}$ and the target view $\mathbf{f}_{\text{warped}}^{(t)}$:

$$\mathbf{C}_{ijk} = \sum_{s \in \mathcal{S}} \sum_h \mathbf{f}_{\text{warped}}^{(t)}(i, j, h) \cdot \mathbf{f}_{\text{warped}}^{(s)}(i, k, h) \quad (2)$$

Here, (i, j, h) and (i, k, h) represent spatial locations and feature channels, with h indexing the concatenated color and depth features, and j and k indexing different spatial positions. The resulting correlation features form a 3D volume \mathbf{C} , which is then fed into a lightweight GRU-based update module, referred to as the *DFM* (Depth Refinement Module) in Fig. 2, that iteratively refines the depth prediction [41].

$$D_s^{(t)} = \Phi_{\text{depth}}(\mathbf{C}, \{K_s\}_{s \in \mathcal{S}}; D_s^{(t-1)}), \quad t = 1, \dots, T \quad (3)$$

where $D_s^{(t)}$ denotes the estimated depth map for source view s at iteration t , Φ_{depth} is a lightweight GRU-based update module, and $\{K_s\}_{s \in \mathcal{S}}$ are the camera intrinsics of the source views. At each iteration, the module refines the depth estimate using the previous prediction $D_s^{(t-1)}$ and local correlation slices extracted from the cost volume \mathbf{C} .

3.2. Temporal Pose Stabilization for Feature Guidance

Beyond depth generation, pose features play a crucial role in enhancing the decoding stage for Gaussian parameter prediction. As illustrated in Fig. 2, the heatmap output $\{\mathbf{f}_{\text{pose}}^{(s)}\}_{s \in \mathcal{S}}$ branches into a secondary pathway directed to the pose decoder, whose feature maps are then fused with the corresponding outputs from the depth and image encoders. Together, these fused features form the skip connections (indicated by red arrows) that feed into the decoder,

which adopts a U-Net-style architecture to predict per-pixel Gaussian attributes, including rotation map \mathcal{M}_r , scale map \mathcal{M}_s , and opacity map \mathcal{M}_α . Pose heatmaps serve as a dynamic auxiliary stream, injecting semantic human structural cues into skip connections to reinforce encoder-decoder alignment and preserve structural consistency during occlusion and fine-grained motion. To ensure reliable pose-based guidance in dynamic scenes, we introduce a *Temporal Pose Stabilizer (TPS)* module that processes heatmaps across adjacent frames. Without such filtering, temporal inconsistencies in pose can lead to flickering artifacts, a common issue in prior methods. Inspired by temporal filtering techniques in video-based pose estimation [6, 13], TPS employs a lightweight recurrent mechanism to smooth pose signals and suppress jitter caused by motion or occlusion. This is particularly important for dynamic, non-rigid subjects like humans, where even minor inconsistencies in pose estimates can degrade reconstruction quality (see our ablation study for analysis). Specifically, TPS takes the pose heatmaps from two consecutive frames, denoted as $\mathbf{f}_{\text{pose}}^{(s)}(t)$ and $\mathbf{f}_{\text{pose}}^{(s)}(t-1)$, and applies a temporal filter to obtain a smoothed pose signal $\tilde{\mathbf{f}}_{\text{pose}}^{(s)}(t)$:

$$\tilde{\mathbf{f}}_{\text{pose}}^{(s)}(t) = \omega \cdot \mathbf{f}_{\text{pose}}^{(s)}(t) + (1 - \omega) \cdot \mathbf{f}_{\text{pose}}^{(s)}(t-1) \quad (4)$$

where $\omega \in [0, 1]$ is a blending factor that controls the contribution of the current frame and the previous frame's pose signal. We use the past frame ($t-1$) instead of the future frame ($t+1$) to ensure causality, which is essential for real-time inference and streaming scenarios. This recurrent mechanism ensures that the pose representation is temporally stable and smooth across frames. Importantly, TPS operates as a pre-processing step before pose encoding, preserving the overall structure of the feature fusion and depth estimation modules.

3.3. Pose-Conditioned Loss Objective

Our training objective integrates pose-aware supervision into the standard differentiable rendering framework, enhancing both geometric fidelity and human-centric feature guidance. The overall loss function is defined as:

$$\mathcal{L}_{\text{total}} = \mathcal{L}_{\text{render}} + \mathcal{L}_{\text{depth}} + \mathcal{L}_{\text{pose-fusion}} \quad (5)$$

While prior works [37, 49, 90] typically optimize only for image reconstruction and depth consistency, our formulation explicitly introduces a pose-conditioned feature alignment loss, enabling stronger structural supervision during training. Specifically, the photometric rendering loss $\mathcal{L}_{\text{render}}$ combines pixel-level fidelity and structural similarity between the rendered view \hat{I} and ground-truth I :

$$\mathcal{L}_{\text{render}} = \beta \mathcal{L}_{\text{MAE}}(\hat{I}, I) + \gamma \mathcal{L}_{\text{SSIM}}(\hat{I}, I) \quad (6)$$

where β and γ balance the reconstruction terms. The depth supervision term $\mathcal{L}_{\text{depth}}$ follows an exponentially weighted scheme to encourage consistent depth predictions across multiple decoding stages:

$$\mathcal{L}_{\text{depth}} = \sum_{t=1}^T \mu^{T-t} \|d_t - d_{\text{gt}}\|_1 \quad (7)$$

where d_t denotes the predicted depth at stage t , d_{gt} is the ground-truth depth, and μ controls the decay rate. Finally, the pose-fusion loss $\mathcal{L}_{\text{pose-fusion}}$ supervises intermediate feature decoding by aligning the fused features f_{joint} —which result from integrating both visual and pose cues—with the pose-encoded features f_{pose} :

$$\mathcal{L}_{\text{pose-fusion}} = \lambda \|f_{\text{joint}} - f_{\text{pose}}\|_1 \quad (8)$$

This term ensures that essential human-centric structural priors, captured by the pose encoder, are preserved throughout decoding. By enforcing this alignment, the model learns to retain and propagate pose-aware semantics, enhancing spatial reasoning in the 3D reconstruction.

4. Experiment Results

System Setup for Runtime Performance All experiments were conducted on a workstation with an AMD Ryzen 9 5900X CPU, 64 GB RAM, and an NVIDIA RTX 4080 GPU (16 GB VRAM). All input images are resized to 512×512 pixels, and our pipeline achieves interactive performance with a per-frame processing time of approximately 100 milliseconds. The end-to-end processing is decomposed as follows: the Gaussian Splatting (GS) rendering module consumes ~ 38 ms; pose feature extraction using a lightweight pose encoder takes ~ 12 ms; image feature extraction via a ResNet-based backbone requires ~ 20 ms; and our Temporal Pose Stabilizer (TPS), which adjusts view blending based on inter-frame pose dynamics, contributes ~ 18 ms. The remaining ~ 12 ms accounts for view-dependent shading, memory overhead, and post-processing (e.g., alpha blending and tone mapping).

Model Specification: We build our method upon a U-Net architecture tailored to multi-scale feature preservation and uncertainty-aware prediction. All training configurations, implementation details, and hardware specifications are provided in the *Appendix*. Our model uses three parallel encoders, each beginning with a 3×3 convolution (32 channels), followed by six residual units with progressively increasing widths (32, 64, 96, 128). Each residual block incorporates a Squeeze-and-Excitation (SE) module for channel-wise attention [21]. Skip connections align encoder and decoder features to preserve multi-scale information. The decoder upsamples the features and outputs three heads: (1) an SR-Opacity head predicting Gaussian



Figure 3. Challenging cases in pose synthesis. Top: occlusion scenario revealing difficult views of hidden regions (e.g., back, inner arms). Bottom: fast motion scenario comparing recent NeRF- and Gaussian-based methods (see Fig. 1 for references)

parameters—scale (3 channels, Softplus), rotation (3 channels, normalized), and opacity (2 channels, Sigmoid); (2) a depth head for auxiliary supervision; and (3) a confidence head for per-pixel uncertainty. The final prediction $\hat{\mathbf{G}}(x)$ is a blend of the predicted output $\mathbf{G}_{\text{dec}}(x)$ and prior $\mathbf{G}_{\text{prior}}(x)$, modulated by the confidence maps $\mathbf{c}(x)$:

$$\hat{\mathbf{G}}(x) = \sigma(\mathbf{c}(x)) \cdot \mathbf{G}_{\text{dec}}(x) + (1 - \sigma(\mathbf{c}(x))) \cdot \mathbf{G}_{\text{prior}}(x) \quad (9)$$

where $\mathbf{c}(x)$ is a learned confidence map. A broader discussion of uncertainty-aware blending strategies can be found in [32].

4.1. Comparison to State-of-the-arts

We evaluate *PoseGaussian* on several public benchmarks for dynamic human reconstruction, including controlled multi-view studio datasets (e.g., ZJU-MoCap) and large-scale benchmarks with diverse poses and motions (e.g., THuman2.0, HuMMan, DNA-Rendering).

ZJU-MoCap					Twindom				
Method	PSNR↑	SSIM↑	LPIPS↓	Train/FPS	Method	PSNR↑	SSIM↑	LPIPS↓	
PixelNeRF [CVPR'21] [81]	24.71	0.892	0.120	1h / 1.20	KeypointNeRF [ECCV'22] [45]	19.68	0.890	-	
NHP [NIPS'21] [35]	28.25	0.955	0.065	1h / 0.15	PixelHuman [arXiv'23] [66]	24.20	0.948	-	
NB [CVPR'21] [54]	29.03	0.964	0.043	10h / 1.48	3D-GS [ACMTOG'23] [33]	22.77	0.785	0.153	
AN [CVPR'21] [52]	29.77	0.965	0.470	10h / 1.11	FloRen [SIGGRAPH'22] [63]	22.96	0.838	0.165	
AS [TPAMI'24] [92]	30.38	0.975	0.037	10h / 0.40	IBRNet [CVPR'21] [72]	22.92	0.803	0.238	
ENeRF [SIGGRAPH'22] [40]	28.90	0.967	-	-	Ours	24.28	0.959	0.101	
HuMMan									
Method	PSNR↑	SSIM↑	LPIPS↓						
HumanNeRF [arXiv'22] [78]	30.66	0.969	0.033	10h / 0.30	NHP[NIPS'21] [35]	18.99	0.845	0.182	
DVA [SIGGRAPH'22] [61]	29.45	0.956	0.038	1.5h / 16.5	MPS-NERF [SIGGRAPH'22] [40]	17.44	0.824	0.193	
InstantNVR [CVPR'23] [17]	31.01	0.971	0.038	5m / 2.20	SHERF [ICCV'23] [22]	20.83	0.891	0.125	
InstantAvatar [CVPR'23] [29]	29.73	0.938	0.068	3m / 4.15	GHG [arXiv'24] [8]	23.86	0.952	0.0591	
KeypointNeRF [ECCV'22] [45]	25.03	0.898	0.104	20h / 1.05	GST [arXiv'24] [57]	18.40	0.87	0.14	
SparseHumanNeRF [CVPR'22] [88]	30.24	0.9679	-	-	Ours	22.18	0.977	0.060	
DNA-Rendering									
Method	PSNR↑	SSIM↑	LPIPS↓						
FlexNeRF [CVPR'23] [26]	31.73	0.9767	0.29	-	HuGS [CVPR'24] [47]	31.5	0.98	0.022	
MonoHuman [CVPR'23] [82]	30.05	0.9684	0.031	-	DVA [SIGGRAPH'22] [61]	29.8	0.97	0.025	
Sem-Human [arXiv'23] [84]	30.80	0.967	0.033	-	ENeRF [SIGGRAPH'22] [40]	28.108	0.972	0.056	
SMPLPix [WACV'21] [56]	27.00	0.91	0.090	-	IBRNet [SIGGRAPH'23] [1]	27.844	0.967	0.081	
GP-NeRF [ECCV'22] [10]	28.80	0.9408	0.090	20h / 1.05	Im4D [SIGGRAPH'23] [39]	28.991	0.973	0.062	
AniNeRF [CVPR'21] [52]	24.56	0.89	0.12	-	4K4D [CVPR'24] [80]	31.173	0.976	0.055	
INR [TPAMI'23] [54]	30.54	0.970	-	-	Ours	30.18	0.989	0.012	
People-Snapshot									
Method	PSNR↑	SSIM↑	LPIPS↓						
HumanSplat [NIPS'24] [48]	29.82	0.9396	0.1048	-	HumanNeRF [arXiv'21] [78]	26.90	0.9605	0.018	
GPS-Gaussian [CVPR'24] [90]	29.68	0.95	-	-	Neural Dressing [CVPR'21] [18]	-	0.91	0.07	
Deform3GS [SIGGRAPH'22] [40]	24.10	0.869	0.126	-	InstantAvatar [CVPR'23] [17]	29.53	0.9716	0.016	
GoMAvatar [CVPR'24] [76]	30.37	0.9689	0.032	23m / 4.15	Anim-NeRF [arXiv'21] [9]	29.37	0.970	0.017	
HuGS [CVPR'24] [47]	26.58	0.934	0.022	-	Neural Body [CVPR'21] [54]	25.49	0.928	-	
SplatArmor [arXiv'23] [27]	30.24	-	0.032	-	GoMAvatar [CVPR'24] [76]	30.68	0.9767	0.0213	
3DGS-Avatar [CVPR'24] [59]	30.61	0.9703	-	30m / 20	SelfRecon [CVPR'22] [28]	24.91	-	0.061	
Deform 3D [arXiv'23] [30]	29.28	0.964	0.040	-	SMPLPix [WACV'21] [56]	17.90	-	0.165	
HUGS [CVPR'24] [34]	30.54	0.970	0.030	-	FlexNeRF [CVPR'23] [26]	28.77	0.904	0.035	
GauHuman [CVPR'24] [23]	31.34	0.965	0.031	1m / 189	SplatArmor [arXiv'23] [27]	27.08	-	0.43	
GART [CVPR'24] [36]	32.22	0.977	0.29	-	GART [CVPR'24] [36]	30.40	0.976	0.037	
Ours	30.86	0.979	0.028	30m / 100	Ours	32.86	0.98	0.014	

Table 1. Comparison of methods on ZJU-MoCap [54], Twindom [71], HuMMan [7], DNA-Rendering [11] and People-Snapshot [2] datasets.

Baseline Evaluation Protocols and Setup Standardization To ensure fair comparison across baselines with differing protocols, we re-implemented or adapted methods to match our pipeline, using official pretrained models or public code when available. The testing setup was unified by fixing 8 input views uniformly sampled across the rig, unlike HumanNeRF [78] (which omits Camera 1) and InstantNVR [17] (which omits Camera 4). All methods used the same temporal sequences and test splits, and evaluation metrics were computed from the same view across methods for alignment; when pretrained models could not be re-evaluated due to dependency or training complexity, we reported published results verbatim and noted protocol differences. For baselines lacking perceptual metrics such as LPIPS, we attempted to re-run their released models; when

not feasible, we marked metrics as unavailable. Since baselines differ in input modality—HumanNeRF [78], InstantNVR [17], and MonoHuman [82] use monocular video, while GPS-Gaussian [90] and NHP [35] rely on multi-view images—we adapted monocular methods by extracting single-camera trajectories from our multi-view dataset, ensuring compatibility.

Quantitative Benchmark Comparison: Table 1 presents a comprehensive quantitative evaluation of our method against state-of-the-art approaches across a diverse set of public benchmark datasets. By leveraging pose as guidance, our method consistently achieves superior structural consistency, attaining the highest SSIM scores across all datasets—including a peak score of 0.979 on ZJU-MoCap [54]. The integration of structural cues and tem-

poral consistency further enhances perceptual quality, as reflected by favorable LPIPS scores ranging from 0.014 to 0.101, underscoring the method’s effectiveness in preserving fine appearance details and visual coherence. While our method did not achieve the highest PSNR, it remains competitive, which is reasonable given that PSNR primarily measures pixel-wise differences and may not fully capture perceptual or temporal quality improvements. In addition, Table 2 focuses exclusively on the THuman 2.0 dataset, where 6-view and 8-view settings on selected sequences are employed to construct controlled benchmarks. This targeted analysis enables a more rigorous evaluation under varying view configurations, which is essential for assessing pose-guided novel view synthesis. Across all tested conditions on THuman 2.0, our method consistently outperforms competing methods, achieving an SSIM score of 0.957 and an LPIPS score of 0.031, demonstrating strong generalization and rendering quality.

Qualitative Comparison: We qualitatively compare our approach under two challenging scenarios: self-occlusion and fast motion. The top rows of Fig. 3 illustrate the self-occlusion scenario, where virtual views are rendered from viewpoints significantly different from the front-facing input cameras (shown in the first column of each row), exposing heavily occluded regions such as the back of the person in Scene 1 and the inner arms in Scene 2. The zoomed-in novel views demonstrate that our method better preserves sharp and continuous body contours—particularly along the challenging back and shoulder regions—and maintains structural details such as clear arm separation, whereas competing methods exhibit noticeable blurring and fragmentation. The bottom rows of Fig. 3 evaluate reconstruction quality under varying motion speeds using only six input views to highlight method differences: *Row 1* (slow motion) shows subtle differences, while faster motions in *Rows 2* and *3* reveal artifacts such as floaters around fast-moving hands and arms. Overall, our method produces more stable and coherent results, although minor distortions may still occur under very rapid motion. Many artifacts are significantly reduced with more input views; we deliberately chose a sparse setup to emphasize the challenge and demonstrate robustness, while denser captures yield near artifact-free results.

Temporal Coherence and Motion Stability: To demonstrate the role of pose in enhancing temporal coherence, we conduct a comprehensive evaluation using SSIM, PSNR, and LPIPS. Here, we present SSIM as a representative example. Our evaluation covers 32 motion sequences featuring challenging dynamics such as rapid limb movement. For statistical robustness, we analyze the average and standard deviation of per-frame Δ SSIM, as well as Δ SSIM values averaged across all sequences. As shown in Table 3, our method achieves the lowest $\mu(\Delta\text{SSIM})$ of 0.023 and

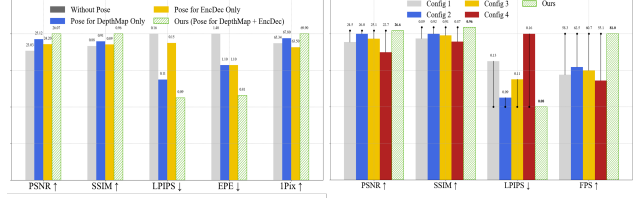


Figure 4. (Left) Impact of pose information. (Right) Impact of pose encoder configurations.

$\sigma(\Delta\text{SSIM})$ of 0.015, almost half of the next best method. This nearly 50% reduction in frame-to-frame SSIM variation translates to visibly smoother and more temporally stable renderings, effectively suppressing the jitter and flickering artifacts commonly observed in competing methods.

4.2. Ablation Study

Fusion Strategies: We explored several fusion strategies to combine the outputs $\{\mathbf{f}_{img}^{(s)}\}_{s \in \mathcal{S}}$ and $\{\mathbf{f}_{pose}^{(s)}\}_{s \in \mathcal{S}}$ from Eq. 1, including concatenation, Feature-wise Attention [86], and Gated Fusion [4]. Feature-wise Attention achieved the best performance, with the lowest EPE (0.75) and 1px accuracy of 78%, at a moderate model size (1.2M parameters). Concatenation offered a favorable trade-off between accuracy and complexity (EPE 0.80, 1px 80%, 0.8M parameters), while Element-wise Addition provided a simpler, more lightweight option (0.5M parameters) but with higher EPE (1.00). Weighted Average Fusion [67] and Element-wise Multiplication also delivered reasonable compromises (EPE \sim 1.1 and 0.98; 0.9–1.0M parameters). More complex methods such as Outer Product Fusion [69] increased parameter counts substantially (1.3–1.8M) with only marginal improvements. Based on these results, we select concatenation as the best balance between accuracy and efficiency.

Loss Hyperparameters: We analyze the effect of the loss weights β , γ , and the pose fusion factor λ through an ablation study, as shown in Table 4. In the absence of pose fusion ($\lambda = 0$), a balanced configuration of RGB and depth losses ($\beta = \gamma = 0.5$) achieves better performance than skewed settings, which trade off perceptual quality for structural accuracy or vice versa. Introducing pose fusion ($\lambda > 0$) consistently improves performance across all metrics. As λ increases, we observe steady gains, with the best results obtained when full pose fusion is applied ($\lambda = 1.0$) along with balanced loss weights.

Pose and Architecture Effects: Fig. 4 illustrates the effects of pose feature integration (left) and network architecture variations (right) on performance. Integrating pose inputs into both the depth map and encoder-decoder pathways delivers the best results, significantly outperforming configurations that incorporate pose in only one component

Method	THuman2.0 Dataset											
	Training						Testing					
	6-camera setup			8-camera setup			Real World Data			Rendered Data		
Method	PSNR↑	SSIM↑	LPIPS↓	PSNR↑	SSIM↑	LPIPS↓	PSNR↑	SSIM↑	LPIPS↓	PSNR↑	SSIM↑	LPIPS↓
3D-GS [ACMTOG'23] [33]	-	-	-	-	-	-	22.97	0.839	0.125	24.18	0.821	0.144
FloRen [SIGGRAPH'22] [63]	18.72	0.770	0.267	23.26	0.812	0.184	22.80	0.872	0.136	23.26	0.812	0.184
IBRNet [CVPR'21] [72]	21.08	0.790	0.263	23.38	0.836	0.212	22.63	0.852	0.177	23.38	0.836	0.212
NARF [SIGGRAPH'22] [40]	-	-	-	-	-	-	21.80	0.8088	-	-	-	-
PIFu [ICCV'19] [62]	-	-	-	-	-	-	-	-	-	20.40	0.921	0.079
ENeRF [SIGGRAPH'22] [40]	21.78	0.831	0.181	24.10	0.869	0.126	23.26	0.893	0.118	24.10	0.869	0.126
SHERF [ICCV'23] [22]	-	-	-	-	-	-	24.26	0.91	0.11	-	-	-
Contex-Human [CVPR'24] [16]	-	-	-	-	-	-	-	-	-	21.40	0.923	0.063
DoubleField [CVPR'22] [64]	-	-	-	-	-	-	25.10	0.905	-	-	-	-
GPS-Gaussian [CVPR'24] [90]	23.03	0.884	0.168	25.57	0.898	0.112	24.64	0.917	0.088	25.57	0.898	0.112
FreeSplat [NIPS'24] [73]	23.35	0.843	0.184	-	-	-	25.90	0.808	0.252	-	-	-
RoGSplat[arXiv'25] [79]	23.12	0.8980	0.1661	-	-	-	25.99	0.9452	0.057	-	-	-
HumanSplat [NIPS'24] [48]	-	-	-	-	-	-	-	-	-	24.033	0.918	0.055
LiFe-GoM [arXiv'25] [75]	-	-	-	24.65	-	0.110	25.32	-	0.099	-	-	-
SIFU [CVPR'24] [87]	-	-	-	-	-	-	-	-	-	22.102	0.923	0.079
HumanSGD [SIGGRAPH'23] [1]	-	-	-	-	-	-	-	-	-	17.365	0.895	0.130
TeCH [3DV'24] [24]	-	-	-	-	-	-	-	-	-	25.211	0.936	0.083
Ours	24.9	0.94	0.09	26.07	0.927	0.081	25.47	0.966	0.05	25.78	0.957	0.031

Table 2. Comparison of methods on the THuman2.0 test set using 6-camera and 8-camera setups, covering both Real World and Rendered data.

Method	$\mu(\Delta\text{SSIM})$	$\sigma(\Delta\text{SSIM})$
3DGS [33]	0.052	0.039
IBRNet [72]	0.0451	0.035
GPS-Gaussian [90]	0.040	0.028
Ours	0.023	0.015

Table 3. Frame-to-frame ΔSSIM consistency.

β	γ	λ	PSNR	SSIM	LPIPS
0.5	0.5	0.0	19.9	0.879	0.205
0.3	0.7	0.0	19.6	0.871	0.212
0.8	0.2	0.0	20.3	0.865	0.225
0.5	0.5	0.1	21.7	0.890	0.180
0.5	0.5	0.5	25.1	0.905	0.148
0.5	0.5	1.0	24.9	0.940	0.090

Table 4. Ablation study of loss hyperparameters β , γ , and pose fusion weight λ on the THuman2.0 dataset.

or omit it altogether. This integration notably enhances perceptual quality, improving the LPIPS score by 45% (0.09 vs. 0.16) compared to the model without pose information. For network design, we evaluated four alternative architecture variants—detailed in the Appendix—that explore the use of Batch Normalization, Residual Blocks, and down-sampling layers. Their performance is summarized in Fig. 4 (right). These ablation studies unequivocally demonstrate that the integration of pose information at both the geometric and feature-encoding stages is critical to the superior

performance of PoseGaussian.

5. Conclusion

We demonstrate that leveraging pose as a structural prior combined with temporal constraints enables our method to achieve state-of-the-art performance on standard benchmarks across multiple public datasets. PoseGaussian effectively reduces motion-induced artifacts in dynamic human scenes, resulting in superior temporal coherence and visual stability in novel view synthesis. While our approach significantly improves reconstruction quality under challenging fast motions, some artifacts persist, especially when the virtual viewpoint shifts considerably from the original capture. Future work will extend our framework to handle multiple interacting people, addressing challenges in occlusion, interaction modeling, and temporal consistency to further enhance reconstruction fidelity in complex dynamic scenes.

References

- [1] Badour AlBahar, Shunsuke Saito, Hung-Yu Tseng, Changil Kim, Johannes Kopf, and Jia-Bin Huang. Single-image 3d human digitization with shape-guided diffusion. In *SIGGRAPH Asia 2023 Conference Papers*, pages 1–11, 2023. 6, 8
- [2] Thimo Alldieck, Marcus Magnor, Weipeng Xu, Christian Theobalt, and Gerard Pons-Moll. Video based reconstruction of 3d people models. In *Proceedings of the IEEE Conference on Computer Vision and Pattern Recognition*, pages 8387–8397, 2018. 6
- [3] Dragomir Anguelov, Praveen Srinivasan, Daphne Koller, Sebastian Thrun, Jim Rodgers, and James Davis. SCAPE:

Shape completion and animation of people. In *ACM SIGGRAPH 2005 Papers*, pages 408–416. ACM, 2005. 2

[4] John Arevalo, Thamar Solorio, Manuel Montes-y Gómez, and Fabio A González. Gated multimodal units for information fusion. *arXiv preprint arXiv:1702.01992*, 2017. 7

[5] Valentin Bazarevsky, Ivan Grishchenko, Karthik Raveendran, Tyler Zhu, Fan Zhang, and Matthias Grundmann. Blazepose: On-device real-time body pose tracking, 2020. 3, 4

[6] Gedas Bertasius, Christoph Feichtenhofer, Du Tran, Jianbo Shi, and Lorenzo Torresani. Learning temporal pose estimation from sparsely labeled videos. In *Advances in Neural Information Processing Systems*, 2019. 4

[7] Zhongang Cai, Daxuan Ren, Ailing Zeng, Zhengyu Lin, Tao Yu, Wenjia Wang, Xiangyu Fan, Yang Gao, Yifan Yu, Liang Pan, et al. Humman: Multi-modal 4d human dataset for versatile sensing and modeling. In *European Conference on Computer Vision*, pages 557–577. Springer, 2022. 6

[8] Jinnan Chen, Chen Li, Jianfeng Zhang, Lingting Zhu, Buzhen Huang, Hanlin Chen, and Gim Hee Lee. Generalizable human gaussians from single-view image. *arXiv preprint arXiv:2406.06050*, 2024. 6

[9] Jianchuan Chen, Ying Zhang, Di Kang, Xuefei Zhe, Linchao Bao, Xu Jia, and Huchuan Lu. Animatable neural radiance fields from monocular rgb videos. *arXiv preprint arXiv:2106.13629*, 2021. 6

[10] Mingfei Chen, Jianfeng Zhang, Xiangyu Xu, Lijuan Liu, Yujun Cai, Jiashi Feng, and Shuicheng Yan. Geometry-guided progressive nerf for generalizable and efficient neural human rendering. In *ECCV*, 2022. 2, 6

[11] Wei Cheng, Ruixiang Chen, Siming Fan, Wanqi Yin, Keyu Chen, Zhongang Cai, Jingbo Wang, Yang Gao, Zhengming Yu, Zhengyu Lin, et al. Dna-rendering: A diverse neural actor repository for high-fidelity human-centric rendering. In *Proceedings of the IEEE/CVF International Conference on Computer Vision*, pages 19982–19993, 2023. 6

[12] Arnab Dey, Cheng-You Lu, Andrew I. Comport, Srinath Sridhar, Chin-Teng Lin, and Jean Martinet. Hfgaussian: Learning generalizable gaussian human with integrated human features, 2024. 2

[13] Runyang Feng, Yixing Gao, Xueqing Ma, Tze Ho Elden Tse, and Hyung Jin Chang. Mutual information-based temporal difference learning for human pose estimation in video. In *Proceedings of the IEEE/CVF Conference on Computer Vision and Pattern Recognition (CVPR)*, pages 17131–17141, 2023. 4

[14] J. Flynn, I. Neulander, J. Philbin, and N. Snavely. Deep-stereo: Learning to predict new views from the world’s imagery. In *Proceedings of the IEEE Conference on Computer Vision and Pattern Recognition (CVPR)*, pages 5515–5524, 2016. 1

[15] Sara Fridovich-Keil, Alex Yu, Matthew Tancik, Qinhong Chen, Benjamin Recht, and Angjoo Kanazawa. Plenoxels: Radiance fields without neural networks. In *Proceedings of the IEEE/CVF Conference on Computer Vision and Pattern Recognition (CVPR)*, pages 5501–5510. IEEE, 2022. 2

[16] Xiangjun Gao, Xiaoyu Li, Chaopeng Zhang, Qi Zhang, Yanpei Cao, Ying Shan, and Long Quan. Contex-human: Free-view rendering of human from a single image with texture-consistent synthesis. In *Proceedings of the IEEE/CVF Conference on Computer Vision and Pattern Recognition*, pages 10084–10094, 2024. 8

[17] Chen Geng, Sida Peng, Zhen Xu, Hujun Bao, and Xiaowei Zhou. Learning neural volumetric representations of dynamic humans in minutes. In *Proceedings of the IEEE/CVF Conference on Computer Vision and Pattern Recognition*, pages 8759–8770, 2023. 2, 6

[18] Artur Grigorev, Karim Iskakov, Anastasia Ianina, Renat Bashirov, Ilya Zakharkin, Alexander Vakhitov, and Victor Lempitsky. Stylepeople: A generative model of fullbody human avatars. In *Proceedings of the IEEE/CVF Conference on Computer Vision and Pattern Recognition (CVPR)*, pages 5151–5160, 2021. 6

[19] Peter Hedman, Pratul P. Srinivasan, Ben Mildenhall, Jonathan T. Barron, and Paul Debevec. Baking neural radiance fields for real-time view synthesis. In *Proceedings of the IEEE/CVF Conference on Computer Vision and Pattern Recognition (CVPR)*, pages 5875–5884. IEEE, 2021. 2

[20] Ming Hou, Jiajia Tang, Jianhai Zhang, Wanzeng Kong, and Qibin Zhao. Deep multimodal multilinear fusion with high-order polynomial pooling. *Advances in Neural Information Processing Systems*, 32, 2019. 4

[21] Jie Hu, Li Shen, and Gang Sun. Squeeze-and-excitation networks. In *Proceedings of the IEEE conference on computer vision and pattern recognition*, pages 7132–7141, 2018. 5

[22] Shoukang Hu, Fangzhou Hong, Liang Pan, Haiyi Mei, Lei Yang, and Ziwei Liu. Sherf: Generalizable human nerf from a single image. In *Proceedings of the IEEE/CVF International Conference on Computer Vision (ICCV)*, pages 9352–9364, 2023. 6, 8

[23] Shoukang Hu and Ziwei Liu. Gauhuman: Articulated gaussian splatting from monocular human videos. In *Proceedings of the IEEE/CVF Conference on Computer Vision and Pattern Recognition (CVPR)*, pages 20418–20431. IEEE, 2024. 1, 2, 3, 6

[24] Yangyi Huang, Hongwei Yi, Yuliang Xiu, Tingting Liao, Jiaxiang Tang, Deng Cai, and Justus Thies. Tech: Text-guided reconstruction of lifelike clothed humans. In *2024 International Conference on 3D Vision (3DV)*, pages 1531–1542. IEEE, 2024. 8

[25] Quang Huynh-Thu and Mahdad Ghanbari. Scope of validity of psnr in image/video quality assessment. *Electronics Letters*, 44(13):800–801, 2008. 2

[26] Vinod Jayasundara, Amit Agrawal, Nicolas Heron, Abhinav Shrivastava, and Larry S. Davis. Flexnerf: Photorealistic free-viewpoint rendering of moving humans from sparse views. In *Proceedings of the IEEE/CVF Conference on Computer Vision and Pattern Recognition (CVPR)*, pages 21118–21127, 2023. 6

[27] Rohit Jena, Ganesh Subramanian Iyer, Siddharth Choudhary, Brandon Smith, Pratik Chaudhari, and James Gee. Splatarmor: Articulated gaussian splatting for animatable humans from monocular rgb videos. *arXiv preprint arXiv:2311.10812*, 2023. 6

[28] Boyi Jiang, Yang Hong, Hujun Bao, and Juyong Zhang. Selfrecon: Self reconstruction your digital avatar from monocular video. In *Proceedings of the IEEE/CVF Conference on Computer Vision and Pattern Recognition*, pages 5605–5615, 2022. 6

[29] Tianjian Jiang, Xu Chen, Jie Song, and Otmar Hilliges. Instantavatar: Learning avatars from monocular video in 60 seconds. In *Proceedings of the IEEE/CVF Conference on Computer Vision and Pattern Recognition*, pages 16922–16932, 2023. 2, 6

[30] HyunJun Jung, Nikolas Brasch, Jifei Song, Eduardo Perez-Pellitero, Yiren Zhou, Zhihao Li, Nassir Navab, and Benjamin Busam. Deformable 3d gaussian splatting for animatable human avatars. *arXiv preprint arXiv:2312.15059*, 2023. 6

[31] Ladislav Kavan, Steven Collins, Jiří Žára, and Carol O’Sullivan. Skinning with dual quaternions. In *Proceedings of the 2007 Symposium on Interactive 3D Graphics and Games (I3D)*, pages 39–46. ACM, 2007. 3

[32] Alex Kendall and Yarin Gal. What uncertainties do we need in bayesian deep learning for computer vision? *NeurIPS*, 2017. 5

[33] Bernhard Kerbl, Georgios Kopanas, Thomas Leimkühler, and George Drettakis. 3d gaussian splatting for real-time radiance field rendering. *ACM Transactions on Graphics (TOG)*, 42(4):1–14, 2023. 1, 2, 6, 8

[34] Muhammed Kocabas, Jen-Hao Rick Chang, James Gabriel, Oncel Tuzel, and Anurag Ranjan. Hugs: Human gaussian splats. In *Proceedings of the IEEE/CVF Conference on Computer Vision and Pattern Recognition (CVPR)*, pages 505–515. IEEE, 2024. 1, 2, 3, 6

[35] Youngjoong Kwon, Dahun Kim, Duygu Ceylan, and Henry Fuchs. Neural human performer: Learning generalizable radiance fields for human performance rendering. *Advances in Neural Information Processing Systems*, 34:24741–24752, 2021. 2, 6

[36] Jiahui Lei, Yufu Wang, Georgios Pavlakos, Lingjie Liu, and Kostas Daniilidis. Gart: Gaussian articulated template models. In *Proceedings of the IEEE/CVF Conference on Computer Vision and Pattern Recognition (CVPR)*, pages 19876–19887, 2024. 6

[37] Mengtian Li, Shengxiang Yao, Zhifeng Xie, and Keyu Chen. Gaussianbody: Clothed human reconstruction via 3d gaussian splatting, 2024. 2, 3, 4

[38] Zhengqi Li, Simon Niklaus, Noah Snavely, and Oliver Wang. Neural scene flow fields for space-time view synthesis of dynamic scenes. In *Proceedings of the IEEE/CVF Conference on Computer Vision and Pattern Recognition (CVPR)*, pages 6498–6508, 2021. 2

[39] Haotong Lin, Sida Peng, Zhen Xu, Tao Xie, Xingyi He, Hujun Bao, and Xiaowei Zhou. High-fidelity and real-time novel view synthesis for dynamic scenes. In *SIGGRAPH Asia 2023 Conference Papers*, pages 1–9, 2023. 6

[40] Haotong Lin, Sida Peng, Zhen Xu, Yunzhi Yan, Qing Shuai, Hujun Bao, and Xiaowei Zhou. Efficient neural radiance fields for interactive free-viewpoint video. In *SIGGRAPH Asia 2022 Conference Papers*, pages 1–9, 2022. 6, 8

[41] Lahav Lipson, Zachary Teed, and Jia Deng. Raft-stereo: Multilevel recurrent field transforms for stereo matching. In *International Conference on 3D Vision (3DV)*, pages 218–227, 2021. 4

[42] Lingjie Liu, Marc Habermann, Vladislav Rudnev, Kiran Sarkar, Jiakai Gu, and Christian Theobalt. Neural actor: Neural free-view synthesis of human actors with pose control, 2021. 2

[43] Rui Xu Liu, Ju Shen, He Wang, Chen Chen, Sen-ching Cheung, and Vijayan Asari. Attention mechanism exploits temporal contexts: Real-time 3d human pose reconstruction. In *Proceedings of the IEEE/CVF Conference on Computer Vision and Pattern Recognition*, pages 5064–5073, 2020. 3

[44] Matthew Loper, Nanyang Mahmood, Javier Romero, Gerard Pons-Moll, and Michael J. Black. Smpl: A skinned multi-person linear model. *ACM Transactions on Graphics (TOG)*, 34(6):1–16, 2015. 1, 2

[45] Marko Mihajlovic, Aayush Bansal, Michael Zollhoefer, Siyu Tang, and Shunsuke Saito. Keypointner: Generalizing image-based volumetric avatars using relative spatial encoding of keypoints. In *European conference on computer vision*, pages 179–197. Springer, 2022. 6

[46] Ben Mildenhall, Pratul P. Srinivasan, Matthew Tancik, Jonathan T. Barron, Ravi Ramamoorthi, and Ren Ng. Nerf: Representing scenes as neural radiance fields for view synthesis. *Communications of the ACM*, 65(1):99–106, 2021. 1, 2

[47] Arthur Moreau, Jifei Song, Helisa Dhamo, Richard Shaw, Yiren Zhou, and Eduardo Pérez-Pellitero. Human gaussian splatting: Real-time rendering of animatable avatars. In *CVPR*, 2024. 2, 3, 6

[48] Panwang Pan, Zhuo Su, Chenguo Lin, Zhen Fan, Yongjie Zhang, Zeming Li, Tingting Shen, Yadong Mu, and Yebin Liu. Humansplat: Generalizable single-image human gaussian splatting with structure priors. In A. Globerson, L. Mackey, D. Belgrave, A. Fan, U. Paquet, J. Tomeczak, and C. Zhang, editors, *Advances in Neural Information Processing Systems*, volume 37, pages 74383–74410. Curran Associates, Inc., 2024. 6, 8

[49] Haokai Pang, Heming Zhu, Adam Kortylewski, Christian Theobalt, and Marc Habermann. Ash: Animatable gaussian splats for efficient and photoreal human rendering. In *Proceedings of the IEEE/CVF Conference on Computer Vision and Pattern Recognition (CVPR)*, pages 1165–1175, 2024. 2, 3, 4

[50] Keunhong Park, Utkarsh Sinha, Jonathan T. Barron, Sofien Bouaziz, Dan B. Goldman, Steven M. Seitz, and Ricardo Martin-Brualla. Nerfies: Deformable neural radiance fields. In *Proceedings of the IEEE/CVF International Conference on Computer Vision (ICCV)*, pages 5865–5874, 2021. 2

[51] Keunhong Park, Utkarsh Sinha, Peter Hedman, Jonathan T. Barron, Sofien Bouaziz, Dan B. Goldman, Ricardo Martin-Brualla, and Steven M. Seitz. Hypernerf: A higher-dimensional representation for topologically varying neural radiance fields, 2021. 2

[52] Sida Peng, Junting Dong, Qianqian Wang, Shangzhan Zhang, Qing Shuai, Xiaowei Zhou, and Hujun Bao. An-

imatable neural radiance fields for modeling dynamic human bodies. In *Proceedings of the IEEE/CVF Conference on Computer Vision and Pattern Recognition (CVPR)*, pages 14314–14323. IEEE, 2021. 2, 6

[53] Sida Peng, Chen Geng, Yuanqing Zhang, Yinghao Xu, Qianqian Wang, Qing Shuai, Xiaowei Zhou, and Hujun Bao. Implicit neural representations with structured latent codes for human body modeling. *IEEE Transactions on Pattern Analysis and Machine Intelligence*, 2023. 2

[54] Sida Peng, Yuanqing Zhang, Yinghao Xu, Qianqian Wang, Qing Shuai, Hujun Bao, and Xiaowei Zhou. Neural body: Implicit neural representations with structured latent codes for novel view synthesis of dynamic humans. In *Proceedings of the IEEE/CVF conference on computer vision and pattern recognition*, pages 9054–9063, 2021. 1, 2, 6

[55] J.-P. Pons, R. Keriven, and O. Faugeras. Multi-view stereo reconstruction and scene flow estimation with a global image-based matching score. *International Journal of Computer Vision*, 72:179–193, 2007. 1

[56] Sergey Prokudin, Michael J Black, Javier Romero, and Sergey Prokudin. Smplpix: Neural avatars from 3d human models. In *Proceedings of the '21*, pages 1810–1819, 2021. 6

[57] Lorenza Prospero, Abdullah Hamdi, Joao F Henriques, and Christian Rupprecht. Gst: Precise 3d human body from a single image with gaussian splatting transformers. *arXiv preprint arXiv:2409.04196*, 2024. 6

[58] Albert Pumarola, Enric Corona, Gerard Pons-Moll, and Francesc Moreno-Noguer. D-nerf: Neural radiance fields for dynamic scenes. In *Proceedings of the IEEE/CVF Conference on Computer Vision and Pattern Recognition (CVPR)*, pages 10318–10327. IEEE, 2021. 1

[59] Zhiyin Qian, Shaofei Wang, Marko Mihajlovic, Andreas Geiger, and Siyu Tang. 3dgs-avatar: Animatable avatars via deformable 3d gaussian splatting. In *Proceedings of the IEEE/CVF Conference on Computer Vision and Pattern Recognition (CVPR)*, 2024. 2, 6

[60] Haoxuan Qu, Li Xu, Yujun Cai, Lin Geng Foo, and Jun Liu. Heatmap distribution matching for human pose estimation. In *Advances in Neural Information Processing Systems (NeurIPS)*, pages 24327–24339. Curran Associates, Inc., 2022. 3

[61] Edoardo Remelli, Timur Bagautdinov, Shunsuke Saito, Changlei Wu, Tomas Simon, Shih-En Wei, Kaiwen Guo, Zhe Cao, Fabian Prada, Jason Saragih, et al. Drivable volumetric avatars using texel-aligned features. In *ACM SIGGRAPH 2022 conference proceedings*, pages 1–9, 2022. 6

[62] Shunsuke Saito, Zeng Huang, Ryota Natsume, Shigeo Morigi, Angjoo Kanazawa, and Hao Li. Pifu: Pixel-aligned implicit function for high-resolution clothed human digitization. In *Proceedings of the IEEE/CVF international conference on computer vision*, pages 2304–2314, 2019. 8

[63] Ruizhi Shao, Liliang Chen, Zerong Zheng, Hongwen Zhang, Yuxiang Zhang, Han Huang, Yandong Guo, and Yebin Liu. Floren: Real-time high-quality human performance rendering via appearance flow using sparse rgb cameras. In *SIGGRAPH Asia 2022 Conference Papers*, pages 1–10, 2022. 6, 8

[64] Ruizhi Shao, Hongwen Zhang, He Zhang, Mingjia Chen, Yan-Pei Cao, Tao Yu, and Yebin Liu. Doublefield: Bridging the neural surface and radiance fields for high-fidelity human reconstruction and rendering. In *Proceedings of the IEEE/CVF Conference on Computer Vision and Pattern Recognition (CVPR)*, pages 15872–15882, 2022. 8

[65] Zhijing Shao, Zhaolong Wang, Zhuang Li, Duotun Wang, Xiangru Lin, Yu Zhang, Mingming Fan, and Zeyu Wang. Splattingavatar: Realistic real-time human avatars with mesh-embedded gaussian splatting. In *Proceedings of the IEEE/CVF Conference on Computer Vision and Pattern Recognition*, pages 1606–1616, 2024. 2, 3

[66] Gyumin Shim, Jaeseong Lee, Junha Hyung, and Jaegul Choo. Pixelhuman: Animatable neural radiance fields from few images. *arXiv preprint arXiv:2307.09070*, 2023. 6

[67] Le Song, Yuchi Lin, Weichang Feng, and Meirong Zhao. A novel automatic weighted image fusion algorithm. In *2009 International Workshop on Intelligent Systems and Applications*, pages 1–4. IEEE, 2009. 4, 7

[68] Shih-Yang Su, Frank Yu, Michael Zollhöfer, and Helge Rhodin. A-nerf: Articulated neural radiance fields for learning human shape, appearance, and pose. In *Advances in Neural Information Processing Systems*, 2021. 1

[69] Fabricio S Terra, Raphael A Viscarra Rossel, and Jose AM Dematte. Spectral fusion by outer product analysis (opa) to improve predictions of soil organic c. *Geoderma*, 335:35–46, 2019. 7

[70] Edgar Tretschk, Ayush Tewari, Vladislav Golyanik, Michael Zollhöfer, Christoph Lassner, and Christian Theobalt. Non-rigid neural radiance fields: Reconstruction and novel view synthesis of a dynamic scene from monocular video. In *Proceedings of the IEEE/CVF International Conference on Computer Vision (ICCV)*, pages 12959–12970. IEEE, 2021. 1

[71] Twindom. Twindom: Full body 3d scanners for 3d printed figurines, 3d portraits, 3d selfies, and avatar products, 2025. 6

[72] Qianqian Wang, Zhicheng Wang, Kyle Genova, Pratul P. Srinivasan, Howard Zhou, Jonathan T. Barron, Ricardo Martin-Brualla, Noah Snavely, and Thomas Funkhouser. Ibr-net: Learning multi-view image-based rendering. In *Proceedings of the IEEE/CVF Conference on Computer Vision and Pattern Recognition (CVPR)*, pages 4690–4699, 2021. 6, 8

[73] Yunsong Wang, Tianxin Huang, Hanlin Chen, and Gim Hee Lee. Freesplat: Generalizable 3d gaussian splatting towards free view synthesis of indoor scenes. In A. Globerson, L. Mackey, D. Belgrave, A. Fan, U. Paquet, J. Tomczak, and C. Zhang, editors, *Advances in Neural Information Processing Systems*, volume 37, pages 107326–107349. Curran Associates, Inc., 2024. 8

[74] Zhou Wang. Image quality assessment: From error visibility to structural similarity. *IEEE Transactions on Image Processing*, 13(4):600–612, 2004. 2

[75] Jing Wen, Alexander G Schwing, and Shenlong Wang. Lifegom: Generalizable human rendering with learned iterative feedback over multi-resolution gaussians-on-mesh. *arXiv preprint arXiv:2502.09617*, 2025. 8

[76] Jing Wen, Xiaoming Zhao, Zhongzheng Ren, Alexander G. Schwing, and Shenlong Wang. Gomavatar: Efficient animatable human modeling from monocular video using gaussians-on-mesh. In *Proceedings of the IEEE/CVF Conference on Computer Vision and Pattern Recognition (CVPR)*, pages 2059–2069, 2024. 6

[77] Chung-Yi Weng, Brian Curless, and Ira Kemelmacher-Shlizerman. Vid2actor: Free-viewpoint animatable person synthesis from video in the wild, 2020. 2

[78] Chung-Yi Weng, Brian Curless, Pratul P. Srinivasan, Jonathan T. Barron, and Ira Kemelmacher-Shlizerman. Hu-manner: Free-viewpoint rendering of moving people from monocular video, 2022. 2, 6

[79] Junjin Xiao, Qing Zhang, Yonewei Nie, Lei Zhu, and Wei-Shi Zheng. Rogsplat: Learning robust generalizable human gaussian splatting from sparse multi-view images. *arXiv preprint arXiv:2503.14198*, 2025. 8

[80] Zhen Xu, Sida Peng, Haotong Lin, Guangzhao He, Jiaming Sun, Yujun Shen, Hujun Bao, and Xiaowei Zhou. 4k4d: Real-time 4d view synthesis at 4k resolution. In *Proceedings of the IEEE/CVF Conference on Computer Vision and Pattern Recognition (CVPR)*, pages 20029–20040, 2024. 6

[81] Alex Yu, Vickie Ye, Matthew Tancik, and Angjoo Kanazawa. pixelnerf: Neural radiance fields from one or few images. In *Proceedings of the IEEE/CVF conference on computer vision and pattern recognition*, pages 4578–4587, 2021. 6

[82] Zhengming Yu, Wei Cheng, Xian Liu, Wayne Wu, and Kwan-Yee Lin. Monohuman: Animatable human neural field from monocular video. In *Proceedings of the IEEE/CVF Conference on Computer Vision and Pattern Recognition (CVPR)*, pages 16943–16953, 2023. 6

[83] Jiakai Zhang, Xinhang Liu, Xinyi Ye, Fuqiang Zhao, Yan-shun Zhang, Minye Wu, Yingliang Zhang, Lan Xu, and Jingyi Yu. Editable free-viewpoint video using a layered neural representation. *ACM Transactions on Graphics (TOG)*, 40(4), 2021. 1, 2

[84] Jie Zhang, Pengcheng Shi, Zaiwang Gu, Yiyang Zhou, and Zhi Wang. Semantic-human: Neural rendering of humans from monocular video with human parsing. *arXiv preprint arXiv:2308.09894*, 2023. 6

[85] Richard Zhang, Phillip Isola, Alexei A Efros, Eli Shechtman, and Oliver Wang. The unreasonable effectiveness of deep features as a perceptual metric. In *Proceedings of the IEEE conference on computer vision and pattern recognition*, pages 586–595, 2018. 2

[86] Sheng Zhang, Min Chen, Jincai Chen, Fuhao Zou, Yuan-Fang Li, and Ping Lu. Multimodal feature-wise co-attention method for visual question answering. *Information Fusion*, 73:1–10, 2021. 7

[87] Zechuan Zhang, Zongxin Yang, and Yi Yang. Sifu: Side-view conditioned implicit function for real-world us-able clothed human reconstruction. In *Proceedings of the IEEE/CVF Conference on Computer Vision and Pattern Recognition*, pages 9936–9947, 2024. 8

[88] Fuqiang Zhao, Wei Yang, Jiakai Zhang, Pei Lin, Yingliang Zhang, Jingyi Yu, and Lan Xu. Humannerf: Efficiently generated human radiance field from sparse inputs. In *Proceed-ings of the IEEE/CVF Conference on Computer Vision and Pattern Recognition (CVPR)*, pages 7743–7753, 2022. 2, 6

[89] Ce Zheng, Sijie Zhu, Matias Mendieta, Taojiannan Yang, Chen Chen, and Zhengming Ding. 3d human pose estimation with spatial and temporal transformers. In *Proceedings of the IEEE/CVF International Conference on Computer Vision (ICCV)*, pages 11656–11665, 2021. 3

[90] Shunyuan Zheng, Boyao Zhou, Ruizhi Shao, Boning Liu, Shengping Zhang, Liqiang Nie, and Yebin Liu. Gps-gaussian: Generalizable pixel-wise 3d gaussian splatting for real-time human novel view synthesis. In *Proceedings of the IEEE/CVF conference on computer vision and pattern recognition*, pages 19680–19690, 2024. 1, 2, 4, 6, 8

[91] T. Zhou, R. Tucker, J. Flynn, G. Fyffe, and N. Snavely. Stereo magnification: Learning view synthesis using multiplane images. In *SIGGRAPH*, 2018. 1

[92] Xiaowei Zhou, Sida Peng, Zhen Xu, Junting Dong, Qianqian Wang, Shangzhan Zhang, Qing Shuai, and Hujun Bao. Animatable implicit neural representations for creating realistic avatars from videos. *IEEE Transactions on Pattern Analysis and Machine Intelligence*, 46(6):4147–4159, 2024. 2, 6